AGU PUBLICATIONS

JGR

Journal of Geophysical Research: Solid Earth

RESEARCH ARTICLE
10.1002/2017JB014573

Key Points:
- Paleoseismic strategy based on fjord sediments
- Well-dated Holocene earthquake history for the Aysén region
- Combining direct and indirect evidence for prehistorical earthquakes

Supporting Information:
- Supporting Information S1
- Table S1

Correspondence to:
K. Wils,
katleen.wils@ugent.be

Citation:
Wils, K., Van Daele, M., Lastras, G., Kissel, C., Lamy, F., & Siani, G. (2018). Holocene event record of Aysén Fjord (Chilean Patagonia): An interplay of volcanic eruptions and crustal and megathrust earthquakes. *Journal of Geophysical Research: Solid Earth*, *123*, 324–343. https://doi.org/10.1002/2017JB014573

Received 16 JUN 2017
Accepted 30 NOV 2017
Accepted article online 13 DEC 2017
Published online 5 JAN 2018

Holocene Event Record of Aysén Fjord (Chilean Patagonia): An Interplay of Volcanic Eruptions and Crustal and Megathrust Earthquakes

Katleen Wils[1], Maarten Van Daele[1], Galderic Lastras[2], Catherine Kissel[3], Frank Lamy[4], and Giuseppe Siani[5]

[1]Renard Centre of Marine Geology (RCMG), Department of Geology, Ghent University, Ghent, Belgium, [2]GRC Geociències Marines, Department of Earth and Ocean Dynamics, Universitat de Barcelona, Barcelona, Spain, [3]Laboratoire des Sciences du Climat et de l'Environnement/IPSL, CEA/CNRS/UVSQ, Université Paris-Saclay, Gif-sur-Yvette, France, [4]Alfred Wegener Institut für Polar- und Meeresforschung, Bremerhaven, Germany, [5]GEOPS, UMR 8148 Université de Paris – Sud 11, Orsay, France

Abstract In the first months of 2007, the Aysén region in southern Chile was affected by a crustal seismic swarm. Its largest earthquake (M_w 6.2) occurred in April and had its epicenter in Aysén Fjord. Seismic intensities became so high that hundreds of onshore mass movements were triggered, several of which entered into the fjord, resulting in mass transport deposits (MTDs) preserved at the fjord bottom. Here we present a Holocene record of paleo-earthquakes in the previously unstudied Patagonian fjordland based on MTD stratigraphy. High-resolution seismic data retrieved using two different seismic systems (sparker and TOPAS) reveal multiple older MTDs on different stratigraphic levels. Correlation of the seismic stratigraphy with sedimentological data obtained from a long Calypso core (MD07-3117) allows conclusion on the seismic origin of these deposits. Additionally, radiocarbon dating permits constructing an age model, validated by tephrochronology, providing an age for the different MTD levels. We thus present a highly detailed paleoseismological history of the Aysén region, including at least six major Holocene earthquakes, one of which is likely related to a known megathrust earthquake. Other earthquakes are related to activity of the Liquiñe-Ofqui Fault Zone (LOFZ), forming the main source of seismic hazard in the area. We can infer a general average recurrence time for LOFZ earthquakes of ~2,100 years in the vicinity of Aysén Fjord with clustered events during the early and late Holocene. Finally, we argue that cascading events (causal link between volcanic and seismic events) may be a frequent phenomenon along the LOFZ.

1. Introduction

The seismic hazard at subduction zones is originating from different source areas. Not only do megathrust earthquakes occur regularly, but intraplate earthquakes such as intra-oceanic and crustal earthquakes are common phenomena as well. Identifying and differentiating the hazard posed by each one of them is required but challenging. Megathrust earthquakes might affect large areas, but large crustal earthquakes can lead to higher seismic intensities close to the epicenter and thus more severe damage, albeit over a more restricted area. Therefore, it is crucial to distinguish between both subduction and other earthquake sources in order to perform an adequate hazard assessment and evaluate which source mechanism forms the most imminent threat for any region in the world.

Chile is known to be one of the most seismically active countries in the world, with regularly occurring earthquakes of moment magnitudes (M_w) exceeding 7 (Lomnitz, 2004), capable of generating intense levels of seismic intensity over very large distances. Many of these large earthquakes originate from the nearby subduction zone running parallel to the Chilean coastline (Figure 1a). For example, the largest instrumentally recorded earthquake is the 1960 Great Chilean earthquake on 22 May, with a M_w of 9.5 and located along the southern part of the subduction zone (Cifuentes, 1989). Another source of natural hazard in the southern part of the country is the Liquiñe-Ofqui Fault Zone (LOFZ) (Hervé, 1976). This forms a prominent structural lineament that runs through the northern Chilean fjordland (Figure 1a). It is an active dextral strike-slip fault (Cembrano et al., 1996), which gave rise to a seismic swarm in 2007. The highest magnitude (M_w 6.2) was reached on 21 April, with an epicenter that was located in Aysén Fjord (Legrand et al., 2011) (Figure 1b). Seismic shaking caused tens of landslides that entered into the fjord and in turn generated large displacement waves or tsunamis with runup heights of several tens of meters (Naranjo et al., 2009).

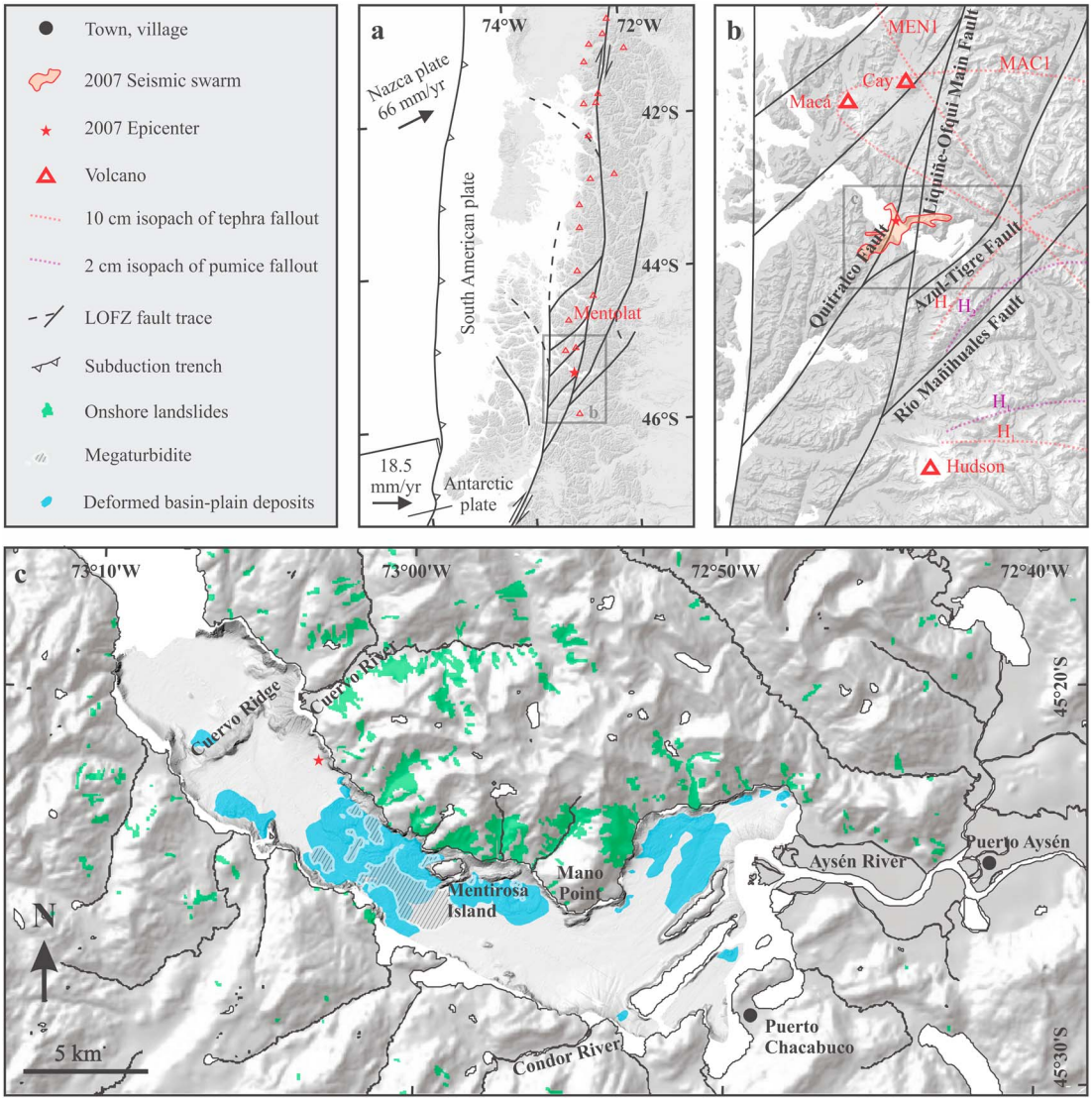

Figure 1. Setting of Aysén Fjord: (a) northern Patagonian fjordland with subduction zone (plate motions from Wang et al., 2007), LOFZ, and volcanoes of south central Chile; (b) region around Aysén Fjord with indication of the Liquiñe-Ofqui Fault Zone (LOFZ) (after Cembrano et al., 2000; Melnick et al., 2009; Thomson, 2002; Vargas et al., 2013), volcanoes in the vicinity of the fjord, tephra, and pumice fallout isopachs of major Holocene eruptions in the area (H = Hudson, MEN = Mentolat and MAC = Macá) (after Naranjo & Stern, 1998, 2004), and the region of the 2007 seismic swarm and main shock (after Legrand et al., 2011; Mora et al., 2010); and (c) shaded relief map of the inner part of the fjord with indication of onshore and offshore mass movements that were triggered by the 2007 main shock of M_w 6.2 on 21 April (after Sepúlveda et al., 2010; Van Daele et al., 2013). Figure adapted from Van Daele et al. (2013).

Landslides and other types of mass transport deposits (MTDs) that enter into a basin are bound to make an imprint in the sediments that are present on the bottom of that basin. Thousands of years later, these imprints can remain preserved in the sedimentary infill of the basin. MTDs have proven to be useful for reconstructing the earthquake history in both lake and fjord settings in several different locations throughout the world such as France, Norway, Chile, Switzerland, and Canada (e.g., Beck, 2009; Bøe et al., 2004; Moernaut et al., 2007; Monecke et al., 2004; Praet et al., 2017; St-Onge et al., 2012; Van Daele et al., 2015). In some cases, observed MTDs in lakes and other basins could even be attributed to major prehistorical earthquakes linked to activated faults (Carrillo et al., 2008; McHugh et al., 2006). Moreover, epicenter locations and magnitudes of the responsible earthquakes have been estimated based on the appearance of simultaneously deposited landslides in different lakes (Kremer et al., 2017; Strasser et al., 2006). In many cases, these studies combine sediment cores with high-resolution seismic data, allowing identification, mapping, and dating of MTDs, as well as determination of their geographical and temporal distribution.

Several records of megathrust earthquakes in south central Chile have been established (Cisternas et al., 2005, 2017; Kempf et al., 2017; Moernaut et al., 2014, 2018), while knowledge of activity on the LOFZ is restricted to recent seismic swarms such as the one in 2007 as well as an event documented in 1927. The latter is known to have caused tsunamis in the region but remains obscure in all other aspects (Naranjo et al., 2009). Historical records only date back to about 100 years ago, which is even less than the already short time span of 500 years that is available in central Chile. There is one study on prehistorical fault activity at Lago Fagnano (Waldmann et al., 2011) in the southern tip of Argentina, but this lake is located in a different tectonic setting. Therefore, there is up to now no way in determining imminent seismic hazard in the LOFZ region.

Due to its location along the Chilean subduction zone and the LOFZ, and because several mass movements were observed there during the 2007 seismic swarm, Aysén Fjord was the subject of prior studies, revealing its potential for paleoseismological reconstructions (Lastras et al., 2013; Van Daele et al., 2013; Vargas et al., 2013). However, these studies were not sufficiently detailed due to the lack of a long sediment core and a limited seismic network, and more detailed research was needed to reveal the seismic history of the Aysén region. The area holds several different fault traces of the LOFZ, and either of these could have been activated during prehistorical earthquakes. A dense network of high-resolution seismic profiles combined with the analysis of a long sediment core retrieved from the fjord provided sufficient information to obtain the first paleoseismic record of the area, which is a first step for hazard and risk assessment.

2. Setting of Aysén Fjord

The southern part of Chile is characterized by the presence of a large number of fjords, termed the Patagonian fjordland (Figure 1). One of these is Aysén Fjord, fed by several rivers including the Condor River, Cuervo River, and Aysén River. The latter is formed by merging of the Mañihuales and Simpson rivers and is by far the largest of the three. The geology of the area surrounding the fjord is dominated by the North Patagonian Batholith, mainly consisting of granites, granodiorites, diorites, and tonalities. An important part of the catchment of the larger feeding rivers is, however, composed of other lithologies such as basaltic to rhyolitic Quaternary volcanic centers. For example, the catchment areas of the Condor and Cuervo Rivers comprise the Hudson and Macá volcanoes, respectively. The catchment of Aysén River is dominated by both volcanic and sedimentary rocks (Sernageomin, 2002).

2.1. Tectonic and Paleoseismological Characterization

The northern part of the Patagonian fjordland is a tectonically active region located along the Chilean subduction zone (Figure 1a). The latter is subdivided in different segments producing megathrust earthquakes with different recurrence rates and magnitudes. Aysén Fjord is located on the southernmost part of the Valdivia segment (~37–46°S), which produced the 1960 Great Chilean earthquake, the largest instrumentally recorded earthquake worldwide (Barrientos & Ward, 1990; Melnick et al., 2009). Seismic intensities reached about IV in the Aysén region but were much higher (up to VIII) in the northern part of the segment (Lazo Hinrichs, 2008), where most of the fault slip was accommodated (Barrientos & Ward, 1990; Moreno et al., 2009). In addition to the presence of a subduction trench, northern Patagonia is crosscut by the Liquiñe-Ofqui Fault Zone (LOFZ), which accommodates the parallel component of the oblique subduction of the Nazca Plate below the South American Plate. It is a dextral strike-slip structural lineament which is about 1,000 km long (Figure 1a) (Mora et al., 2010, and references therein). Aysén Fjord is crossed by one of the larger fault branches, a horsetail fault termed the Quitralco Fault (Vargas et al., 2013). Other important fault branches in the area are the Azul-Tigre Fault, running along the easternmost side of the fjord, and the Río Mañihuales Fault to the south of the Azul-Tigre Fault, running more or less parallel to the latter (Thomson, 2002) (Figure 1b).

In the first months of 2007, the area around Aysén Fjord was affected by a seismic swarm. The swarm started at the end of January, reached its maximum magnitudes in April with two events with a magnitude larger than 6, and subsequently waned until about mid-June. The first large earthquake (normal faulting) occurred on 2 April with a M_w of 6.1; the largest event (strike slip) of M_w 6.2 took place on the 21st of the same month (Legrand et al., 2011). Most of the seismic network that was installed in the area during the seismic swarm was destroyed due to the tsunamis generated by mass movements entering the fjord at the time of the main shock, making it impossible to determine the hypocenter locations precisely (Lastras et al., 2013;

Naranjo et al., 2009). This explains why different locations are cited by different sources. Legrand et al. (2011) base their hypocenter estimations on the local seismic network and give locations lying in the inner fjord at large depth for the first event and shallow depth for the second. However, Russo et al. (2011) use the same seismic network and place both earthquakes at a shallow depth but with the first shock occurring 50 km further to the west. Despite these differences, it is clear that the M_w 6.1 event was located either too far away or too deep, and therefore only the M_w 6.2 event was able to cause major landslides around the fjord. Intensities recorded around the epicentral zone ranged from VIII to IX and decreased to VII at the eastern side of the fjord (Naranjo et al., 2009). Legrand et al. (2011) propose that the swarm originated from movement of fluids, in this way reactivating motion along the LOFZ (Naranjo et al., 2009). It was hosted by the Quitralco Fault (Vargas et al., 2013). The M_w 6.2 event triggered hundreds of mass movements in the epicentral area along the fjord coastline, including rock falls, rock avalanches, landslides, debris flows, and soil-vegetation slides (Naranjo et al., 2009) of which some of the more voluminous events induced large tsunami waves (Lastras et al., 2013). The distribution of these mass movements in the vicinity of Aysén Fjord is given by Sepúlveda et al. (2010) and visualized in Figure 1c, together with all offshore mass movement deposits observed by Van Daele et al. (2013).

2.2. Volcanic Activity

Volcanism in the Andean Cordillera can be divided into four different zones, which are further divided into smaller segments. The area around Aysén Fjord holds several major Pleistocene-Holocene volcanoes belonging to the southern part of the Andean Southern Volcanic Zone (SVZ, 33–46°S). The most common volcanic rocks that can be found are tholeitic, high-Al basalts, and basaltic andesites. However, also andesites, dacites, and rhyolites can occasionally be found (Stern, 2004, and references therein). The locations of most of the large stratovolcanoes in this part of the Cordillera are controlled by the presence of the LOFZ (Cembrano & Lara, 2009). Macá and Cay volcanoes lie to the north of the fjord, at a distance of about 20 and 30 km, respectively. Mentolat can also be found northward of the fjord but is located 65 km away. About 50 km south of the fjord lies Hudson Volcano (Figure 1b**)**.

Naranjo and Stern (2004) describe the Holocene tephrochronology of the southernmost part of the SVZ. A tephra fall deposit located along the Simpson River with a maximum age of 7,650–7,870 cal years B.P. has been attributed to Mentolat Volcano and is referred to as MEN1. This age range is confirmed by Stern et al. (2016), reporting 7,630–7,750 cal years B.P. in lake cores. The size of the eruption is unknown, but tephra and pumice fallout has been observed in the Aysén River catchment. Other tephra fall deposits have been found to the east of Macá Volcano along the Simpson and Mañihuales River valleys. They have been dated back to maximum 1,300–1,520 cal years B.P. and originate from a small to medium size explosive eruption termed MAC1. Similar to MEN1, material attributed to the MAC1 eruption has been retrieved in the Aysén River catchment. There is no evidence for prehistorical activity of Cay Volcano.

Hudson Volcano has had several large explosive eruptions during the Holocene and is one of the most active volcanoes of the southern Andes. Two of the largest eruptions are termed H1 and H2 and are dated to 7,690–8,720 cal years B.P. (Stern & Weller, 2012) (8,410–8,540 cal years B.P. in lake cores; Stern et al., 2016) and between 3,460 and 4,100 cal years B.P. (Naranjo & Stern, 1998), respectively. The H2 eruption might have even caused fallout in Aysén Fjord (Naranjo & Stern, 1998). Lago Castor, located about 100 km eastward of Aysén Fjord, holds a pumice layer attributed to H2 and was dated to 3,970–4,110 cal years B.P. (Van Daele et al., 2016). Sediment cores from different lakes in the Aysén region show a thick tephra layer of late glacial age, which was attributed to an eruption of Hudson Volcano between 17,075 and 17,605 cal years B.P. referred to as Ho and is assumed to be even larger than H1 and H2 (Weller et al., 2014).

3. Material and Methods

Geophysical data was acquired during a Ghent University survey in December 2009 on board RV *Don Este* (Van Daele et al., 2013) and during the University of Barcelona DETSUFA cruise in March 2013 on board BIO *Hespérides* (Lastras and The Shipboard Scientific Party, 2013). Additionally, a long Calypso core in the inner fjord was retrieved during the PACHIDERME survey on board RV *Marion Dufresne* in February 2007 (i.e., before the 2007 earthquake) (Kissel et al., 2007).

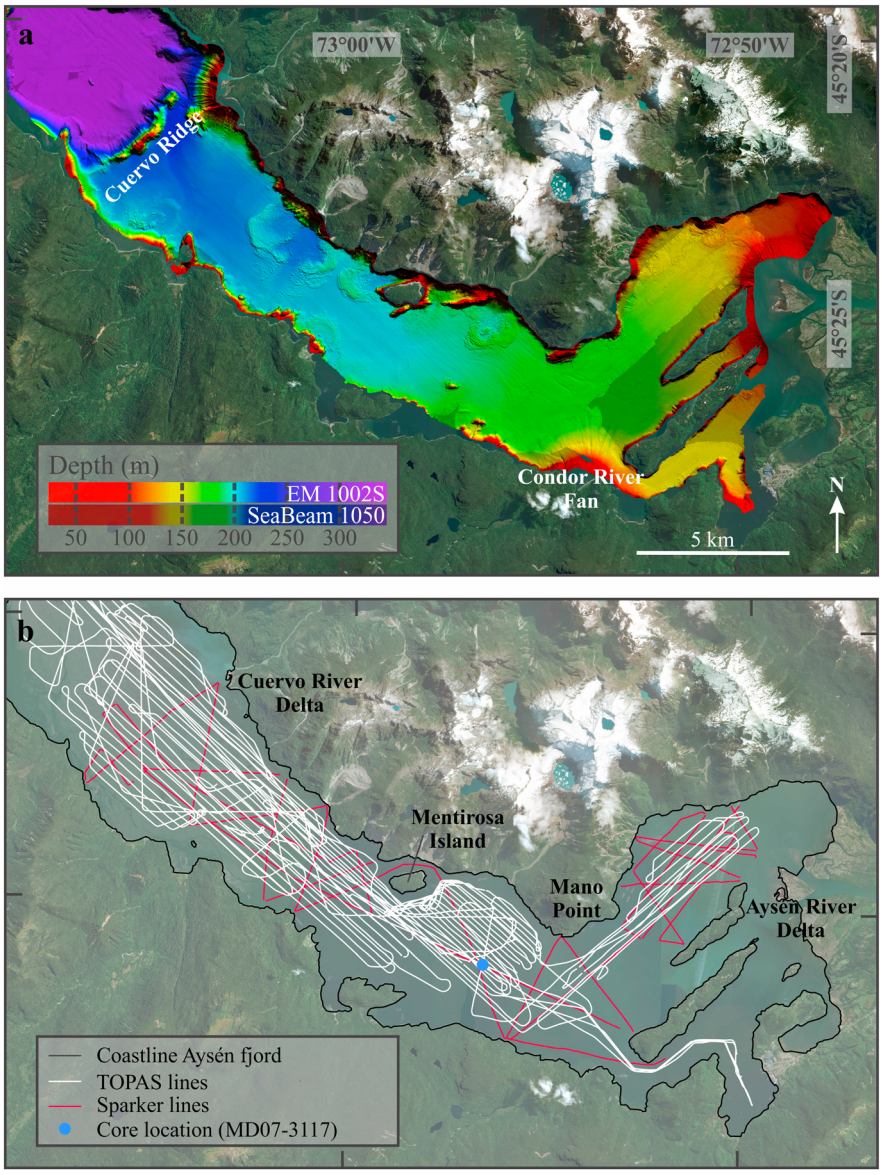

Figure 2. Visualization of all the data used in this study: (a) multibeam bathymetry map combining EM 1002S and SeaBeam 1050 data and (b) high-density seismic network and core (MD07-3117) location, with a satellite image (©DigitalGlobe) from after the 2007 Aysén seismic swarm as background. Both the onshore landslide scars and the deformed basin plain deposits due to the 2007 main shock are evident (compare to Figure 1c).

3.1. Swath Bathymetry

Two types of multibeam data are combined: ELAC SeaBeam 1050 multibeam sonar, which covers a larger area in the inner fjord, and EM 1002S Kongsberg multibeam echosounder, which provides higher resolution in the entire fjord. The former has two 50 kHz transducer arrays and operates with an equiangular beam spacing of 120°, transmitting and receiving at 108 beams of 3 × 3° beam width (Van Daele et al., 2013). The latter has a nominal sonar frequency of 95 kHz using 111 beams of 2 × 2° per ping and operates with an equidistant beam spacing resulting in 150 m swath width (Lastras and The Shipboard Scientific Party, 2013). After processing, the resulting maps were imported in IHS Kingdom Suite software for visualization and integration with seismic reflection data (Figure 2a).

3.2. Seismic Reflection Data

Seismic profiles were acquired using different seismic systems (Figure 2b): a CENTIPEDE multielectrode sparker (0.4–1.5 kHz) for medium resolution and penetration depth in the inner fjord, and a Kongsberg TOPAS

PS18 parametric subbottom profiler (1.5–4.5 kHz) for high-resolution data covering the entire fjord. After some preliminary processing (application of a matched filter, gain control, and seismic attribution of instantaneous amplitude), the seismic lines were imported into IHS Kingdom Suite. For comparison, the TOPAS source has a maximum vertical resolution of about 0.2 ms (corresponding to about 15 cm), while the sparker can only resolve structures of about 50 cm. We identified landslides and (mega)turbidites within the sedimentary infill of the fjord, which could indicate past earthquakes. Sparker profiles have already been interpreted in Van Daele et al. (2013) and serve as a base for further analysis and interpretation of the much closer spaced TOPAS profiles (Figure 2). The terminology of horizons mapped by Van Daele et al. (2013) has been adapted to our interpretations.

3.3. Sediment Core Logging

The stratigraphic position of all event deposits identified in the seismic profiles is traced toward the location of a 21.14 m long Calypso core taken within the fjord (MD07-3117, Figure 2b) and eventually correlated with one of the layers present therein. The core was first logged with the GEOTEK Multi Sensor Core Logger (MSCL) on board the Marion Dufresne for *P* wave velocity, gamma ray attenuation, and magnetic susceptibility (MS) at a 2 cm interval (Kissel et al., 2007). Aiming at identifying turbidites, additional scans were made with the Ghent University GEOTEK MSCL for digital linescan images and high-resolution MS measurements at a 2 mm interval (Bartington MS2E). Sections of the core that clearly contain tephras and/or turbidites were subjected to X-ray computed tomography (CT) scanning at the Ghent University Hospital (Siemens; SOMATOM Definition Flash; Siemens AG, Healthcare Sector, Erlangen, Germany). The scanner was employed at 120 kV, and a rotation time of 1 s was set, resulting in a resolution of ~0.2 mm in the *x* and *y* directions and a *z* resolution of 0.6 mm. VGStudio 2.0 software was used for visualization and analysis of CT volumes.

3.4. Chronology

Organic material distributed throughout the core was radiocarbon dated. In total, 23 samples containing terrestrial macroremains (well-preserved leafs and twigs) were analyzed using the ARTEMIS Accelerator Mass Spectrometry (AMS) facility in Saclay (Moreau et al., 2013). Classical age-depth modeling was done with CLAM (version 2.2; Blaauw, 2010) using the most recent calibration curve for the southern hemisphere (SHCal13; Hogg et al., 2013).

To validate the obtained age model, 10 tephra samples were identified along the core MD07-3117 following the procedure previously described in Carel, Siani, and Delpech (2011). For each sample, selected volcanic glass shards were handpicked, mounted on epoxy resin beads, and polished on an automated polish wheel to avoid compositional variations due to surficial alteration processes. Major-element analyses were performed on CAMECA-SX 100 Electron Microprobe (EPMA-CAMPARIS) at the University Paris VI (France).

4. Results and Interpretation

4.1. Geophysical Data Analysis

In general, multibeam data show a rather flat basin morphology in the inner fjord interrupted by some large positive reliefs (Figure 2a). These reliefs are also clearly visible in seismic profiles as strong seafloor reflectors with a typical chaotic to opaque seismic facies, sometimes associated with a transparent ponding unit filling up the depressions (Figure 3). Van Daele et al. (2013) interpreted these as MTDs and associated megaturbidites, respectively, that are the result of the main shock of the 2007 Aysén seismic swarm. These disturb the regular sedimentation in the fjord, expressed as a horizontal-to-subhorizontal stratified seismic facies. Similar structures can be found buried in the sedimentary infill of the basin and have been identified on 10 stratigraphic levels (SL) along which they are connected via continuous high-amplitude reflectors, from top to bottom: SL-G, SL-F, SL-EF, SL-E, SL-DE, SL-D, SL-CD, SL-C, SL-B, and SL-A. The nomenclature is generally coincident with that published by Van Daele et al. (2013) with the addition of new event layers identified during this research. The MTDs have different morphologies comprising erosive structures, unconfined flow deposits, and local accumulations. Megaturbidites are considered separately, since they effectuate leveling of the basin plain. SL-A, SL-B, SL-C, SL-D, SL-F, and SL-G contain major event deposits, while the remaining levels only show smaller-scale deposits (Figure 4).

The bathymetry data and distribution maps of the different MTDs (Figure 2a, Figure 4) clearly show that the 2007 deposits are distributed over the entire inner fjord. This is not the case for SL-G, with two separate major

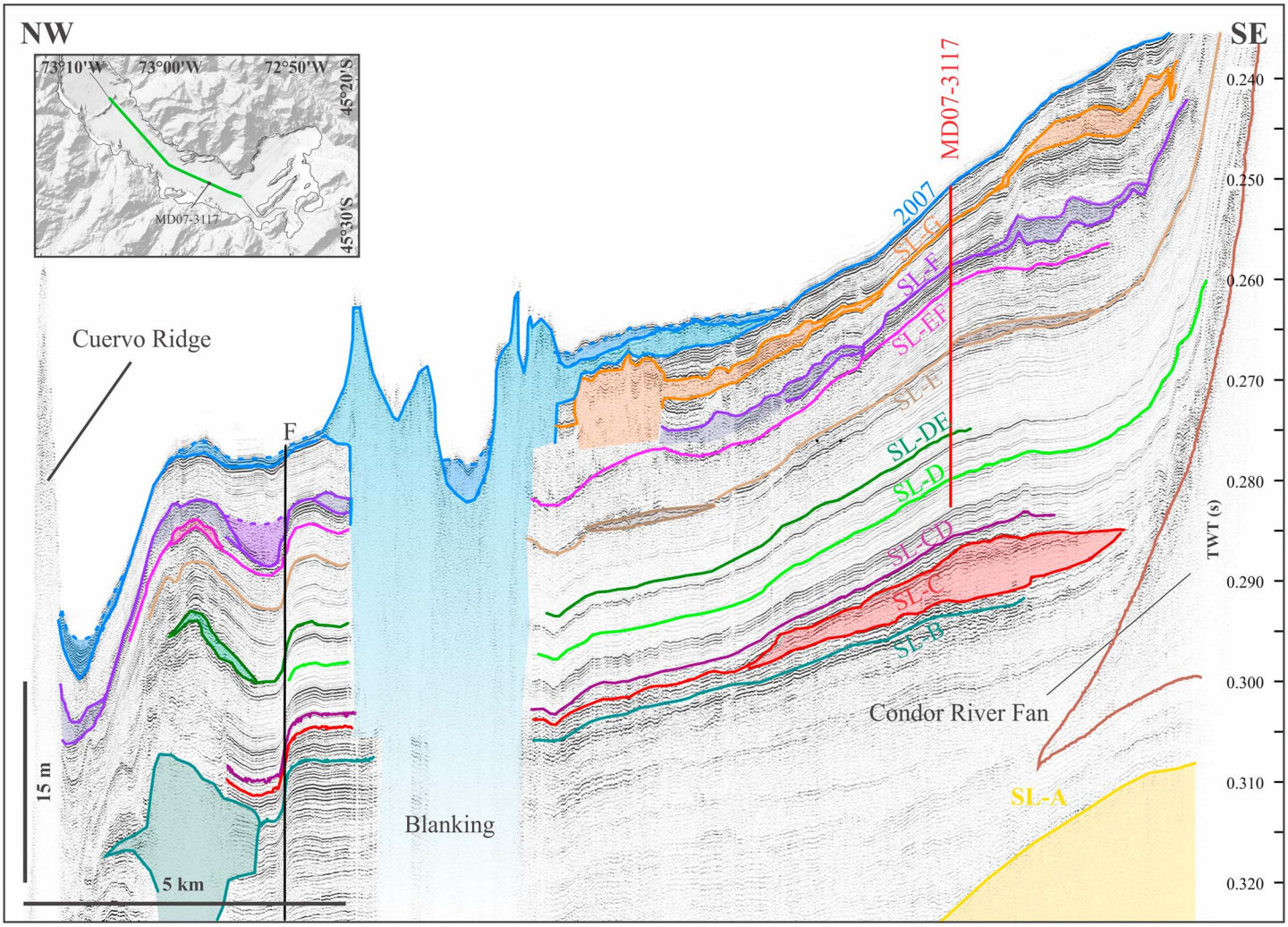

Figure 3. Interpreted TOPAS seismic line 209_000, expressed in two-way travel time (TWT). The location of the profile with respect to the fjord is given in the top left corner. For all stratigraphic levels, MTDs and megaturbidites are both marked with colored areas, with megaturbidites differentiating from MTDs by a dashed line at their top. Where the base of the MTDs cannot be observed, the colored area is not contoured. An extreme case of blanking occurs below the 2007 deposits, preventing the visualization of anything underneath them. The location of MD07-3117 is also marked, together with the expression of the Quitralco fault (F) and the contours of the Condor River fan. For an uninterpreted version of this profile, the reader is referred to Figure S1.

emergent erosive MTDs that gradually evolve into a debris flow deposit in the area between Mentirosa Island and Mano Point and a smaller one close to the Aysén River Delta (Figures 3 and 4). SL-F is more similar to the 2007 event with MTDs throughout the inner fjord. In the area around Mano Point, two individual debris flow-like deposits are stacked directly on top of each other. Additionally, a megaturbidite to the west of Mentirosa Island fills in the depressions between the MTDs. SL-EF consists of relatively small-scale MTDs spread over the area between Cuervo Ridge and Mano Point. A large part of the data in the area of Mentirosa Island up to Mano Point is unclear because of blanking by the SL-F deposits, and only (parts of) small-scale deposits can be identified. SL-E consists of isolated, thin local accumulations of material concentrated in the center of the fjord basin and a seismic reflector that increases in amplitude toward the Condor River fan. Below SL-E lies another event deposit, termed SL-DE, consisting of a few debris flow-like deposits located near the Cuervo Ridge. The next buried event deposits are present at SL-D, showing several erosive and some debris flow-like structures around Mano Point and west of the Condor River fan. Below lies SL-CD, with just one debris flow-like deposit between Mentirosa Island and Mano Point. Due to acoustic blanking by a large amount of rocks in the 2007 deposits originating from onshore (Sepúlveda et al., 2010), the total extent of this deposit cannot be determined. The next stratigraphic level is SL-C, with one debris flow-like deposit around Mano Point with a distribution similar to the one from SL-G. SL-B shows rather large

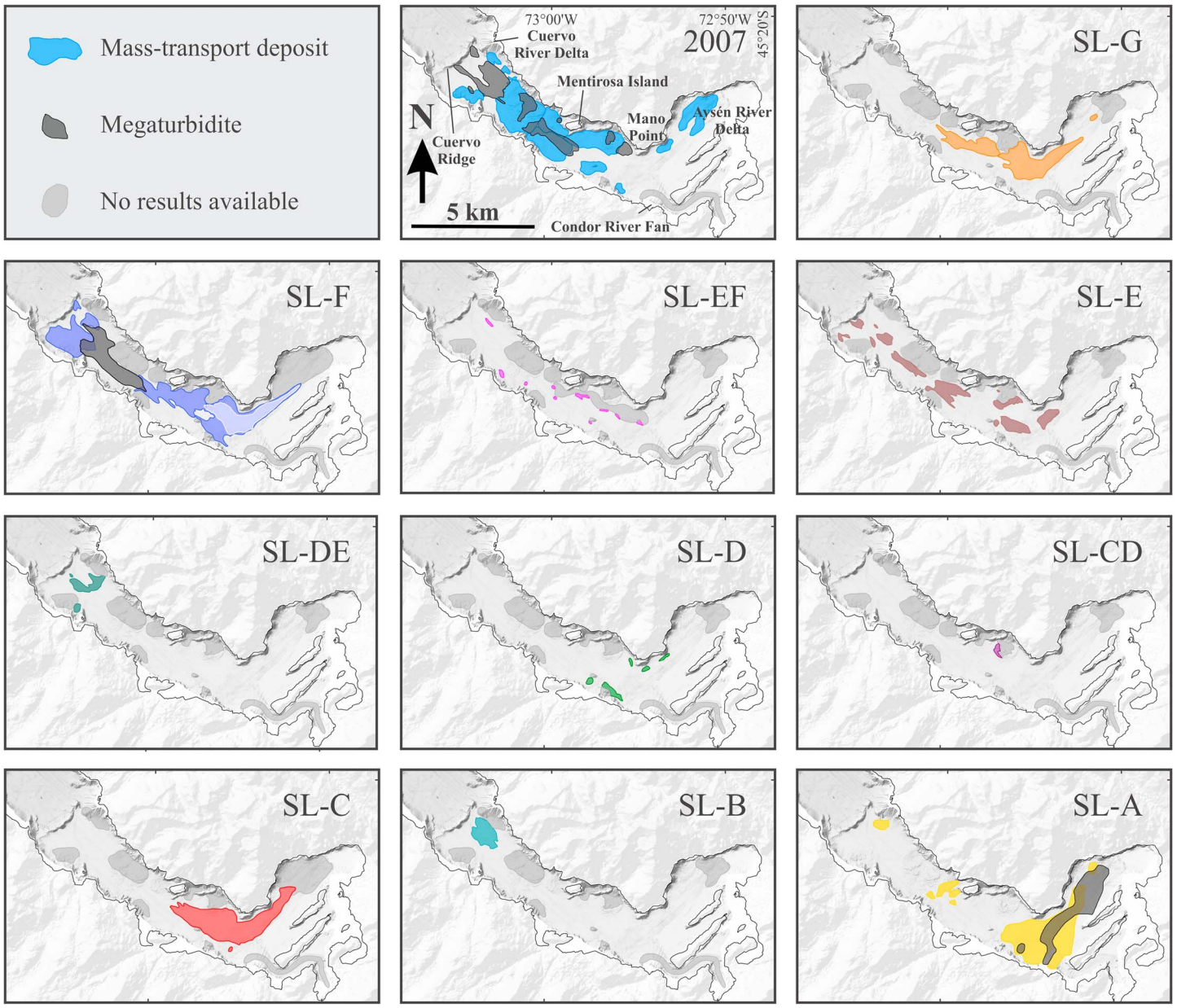

Figure 4. Maps showing the location of the different MTDs (colored areas) and associated megaturbidites (dark gray areas) for each stratigraphic level. MTD colors match those from Figure 3, and areas where no results are available, either because of blanking by overlying event deposits or because the data are unclear, are indicated in light gray. In the case of SL-F, two different deposits with a debris flow-like morphology belong to the same stratigraphic level: the lighter-colored deposit is placed directly on top of the blue one. Note that no information about the sedimentary infill is available for the easternmost part of the fjord, and therefore, the number and distribution of buried events is likely underrepresented.

erosive MTDs near the Cuervo River Delta. The deepest event deposit visible on the seismic profiles is SL-A, with both MTDs and megaturbidites mainly on the eastern side of the fjord but also a small one on the western side, at the Cuervo River Delta. Because of its depth in the stratigraphy and limited thickness, it is only visible on the sparker profiles, which do not cover the entire inner fjord.

Locally, the seismic reflectors show vertical shifts associated with hyperbolic reflections, suggesting the presence of faults. The large fault to the northwest in Figure 3 causes an offset with hyperbolic reflections up to the top of the sediment infill (Figure 5). There is (at maximum) 2 ms vertical offset at the seafloor and is not constant throughout the stratigraphic column. Offset increases at SL-F to ~5 ms, but this 3 ms increase is leveled out by the megaturbidite present in the hanging wall. Further below, the offset remains constant.

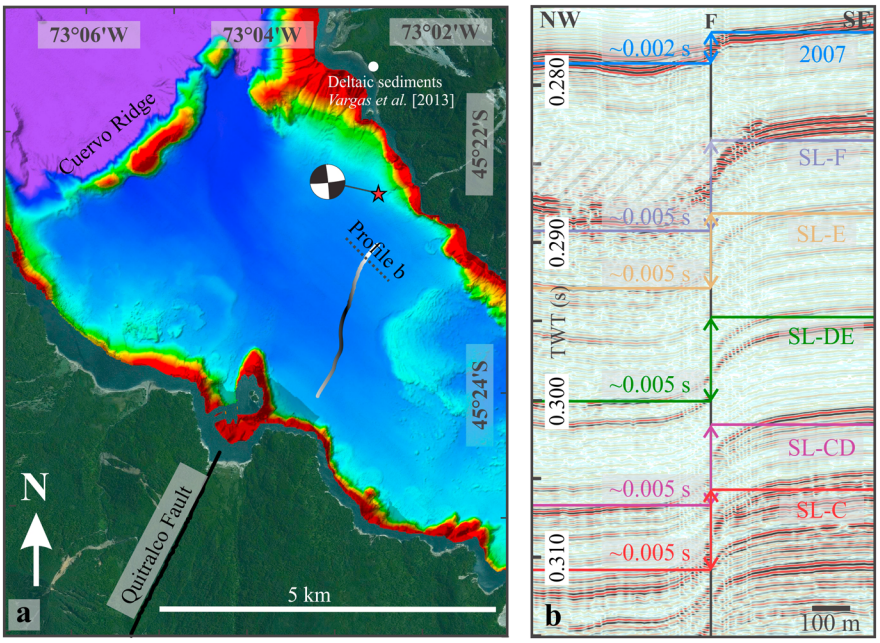

Figure 5. Offshore sedimentary trace of the Quitralco Fault, showing vertical stratigraphic offset. (a) Multibeam bathymetry map where the gray shading of the fault trace represents the offset at the seafloor, which is consistent with "surface" rupture of the bedrock below the fjord's sedimentary infill following the M_w 6.2 earthquake's (epicenter indicated by red star) moment tensor (Legrand et al., 2011): Black, no vertical offset, where fault trace is parallel to along-fault movement; white, largest offset, at an angle with movement along the fault. Location of deltaic sediments dated in Vargas et al. (2013) is indicated (white dot), (b) zoom from part of TOPAS profile 024 (dashed line, where offset is maximal) that shows the seismic expression of the fault, with indication of fault offset values for each stratigraphic level. The shaded area indicates the megaturbidite that levels vertical offset at SL-F.

This indicates that the sediments record at least two earthquakes hosted by this fault. The offset values change along the fault trace for both the surface level and SL-F, becoming less evident toward the south and eventually even shift sense, the hanging wall being on the eastern side instead of the western. Moreover, the southern part never reaches the large offset values of the northern sections and is less than 1 ms for the surface level, SL-F, and below.

4.2. Core Lithology

The MD07-3117 core consists mostly of brown mud with the occasional presence of plant debris and is partly bioturbated. The bottom of the core (~21 m depth) contains rock fragments in muddy sediment. Based on core pictures, MS, gamma ray density, and CT scans, specific intervals with distinct characteristics are identified as event deposits, interrupting the regular sedimentation in the fjord. These event deposits can be either a tephra or a turbidite. Turbidites typically have a high MS and consist of gray granitic or black volcanic sand, possibly rich in organic matter, with a fining upward trend (Van Daele et al., 2014) (e.g., Figure 6c). Moreover, they often show structures indicating flow such as ripples. Sandy layers in a muddy matrix with a very sharp MS peak are considered to be of volcanic origin (e.g., Figure 6e). Halfway in the core a macroscopically identifiable pumice layer of about 35 cm thick is present (Figure 6d). It shows a coarsening upward sequence in the upper 10 cm of the deposit, which we interpret as gradual sinking of floating pumice, a phenomenon observed by (Bertrand et al., 2014). This layer is brighter than the rest of the sediment in the core, just like all other whitish pumice layers. A schematic representation of the core with all of the event deposits (independent of their origin) is shown in Figure 6.

4.3. Construction of an Age-Depth Model

4.3.1. Radiocarbon Dating

Radiocarbon dating (Table 1) allows construction a suitable age-depth model for MD07-3117 core. Our age-depth model is based on the dating of 20 well-preserved leaves and twigs. These terrestrial macroremains are generally considered to have a very limited depositional time lag and therefore provide accurate radiocarbon ages (Bertrand et al., 2012; Björck et al., 1998; Törnqvist et al., 1992). Three samples are not

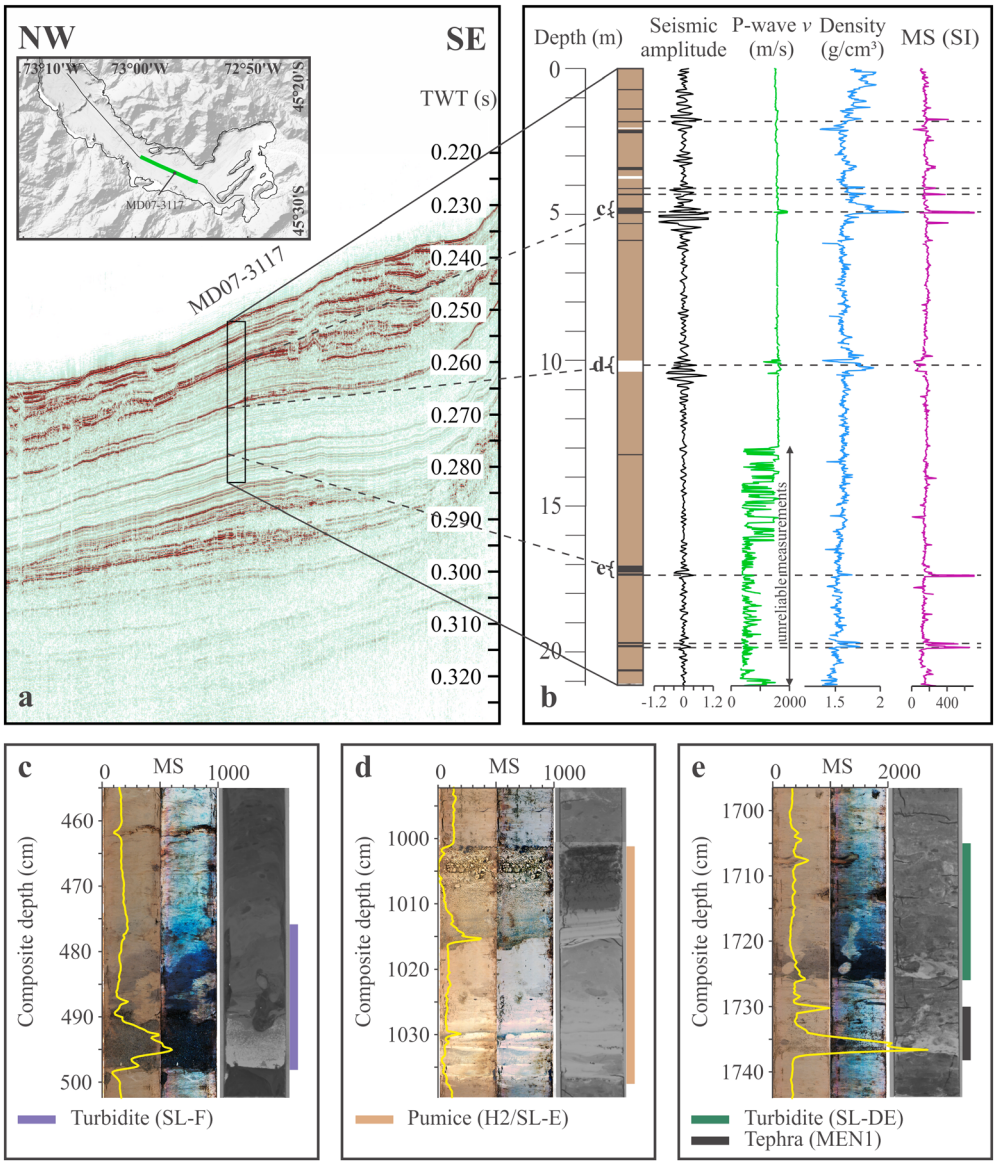

Figure 6. (top row) Correlation between MD07-3117 and the seismic data and (bottom row) visualization of three specific intervals of the core. (a) Extent of the core drawn on TOPAS profile 209_000 (vertical scale in two-way travel time, TWT) with the location of the seismic line and the core with respect to the fjord given in the top left corner; (b) schematic lithology of the core (brown represents mud, black intervals are either a tephra or turbidite, and white are pumice layers) together with a seismic wiggle (black) and MSCL measurements of *P* wave velocity (green), core density (blue), and MS (purple). *P* wave velocity in the bottom 8 m of the core is not correct due to erroneous measurements. (c) Black turbidite, (d) thick pumice layer about halfway in the core, and (e) two event deposits, the upper one is a strongly bioturbated black turbidite, while the lower one is a tephra. For each section three images are given: Real color image (left) with magnetic susceptibility (yellow curve and top scale), histogram equalized color image (middle), and gray scale CT scan cross section (right).

considered in the model due to various reasons. Considering that sample AY-RC1 is located almost at the core top and thus consists of very recent material, it most likely has a post-1950 age (sedimentation rates of 0.19–0.30 cm/yr in the upper 25 cm of sediment on two locations in inner Aysén Fjord imply that the sample cannot be older than 1991; Salamanca & Jara, 2003) and thus is not suitable for calibration with SHCal13 (Hogg et al., 2013). AY-RC5 was taken from within an organic layer in the top of a turbidite (209–221 cm). This sample is considered to be reworked and is therefore not used in the age model. AY-RC20 has a far younger age than samples at a similar depth, which could be the consequence of lab contamination that we suspect to have occurred for this sample. Event deposits (i.e., tephra layers and turbidites) are considered to be instantaneous and are implemented into the model as "slumps."

Table 1
Radiocarbon Samples

Sample number	Total depth (cm)	Dry weight (mg)	Description	^{14}C age (years B.P. ± 1σ)	2σ calibrated age range (min–max, cal years B.P.)
AY-RC1[a]	3	4.4	Branch	490 ± 30	470–535
AY-RC2	67	3.1	Leaf	300 ± 30	156–446
AY-RC3	94.5	12.5	Leaf	225 ± 30	−2–304
AY-RC4	174	2.4	Leaf	605 ± 30	522–632
AY-RC5[a]	213	64.8	Wood	915 ± 30	694–904
AY-RC6	358	6.0	Wood	1,640 ± 30	1,412–1,559
AY-RC7	380	0.9	Leaf	1,615 ± 30	1,379–1,534
AY-RC8	419	1.0	Leaf	1,715 ± 30	1,523–1,699
AY-RC9	467	73.8	Wood	2,100 ± 30	1,930–2,142
AY-RC10	526.5	2.7	Leaf	1,975 ± 45	1,748–2,000
AY-RC11	662	9.2	Leaf	2,585 ± 30	2,491–2,751
AY-RC12	823	5.9	Wood	3,225 ± 30	3,276–3,477
AY-RC13	981.5	21.1	Wood	3,785 ± 30	3,982–4,229
AY-RC14	995.5	2.5	Leaf	3,750 ± 45	3,901–4,225
AY-RC15	1,456	11.2	Leaf	5,250 ± 30	5,904–6,172
AY-RC16	1,499	20.6	Wood	5,520 ± 30	6,197–6,392
AY-RC17	1,572	10.9	Wood	5,920 ± 35	6,567–6,792
AY-RC18	1,751	2.4	Leaf	6,800 ± 35	7,568–7,675
AY-RC19	1,870	11.5	Wood	7,960 ± 40	8,604–8,977
AY-RC20[a]	1,878.5	4.4	Leaf	5,280 ± 30	5,917–6,176
AY-RC21	1,896	5.1	Wood	7,455 ± 40	8,163–8,358
AY-RC22	1,905	1.3	Leaf	7,580 ± 35	8,214–8,414
AY-RC23	2,001	1.2	Wood	8,080 ± 40	8,723–9,030

[a]Samples excluded for age-depth modeling.

Comparison of MD07-3117 with short gravity cores studied by Van Daele et al. (2013) shows that the former's top sediments are complete. A smooth spline curve with a smoothing of 0.5 is applied (Telford, Heegaard, & Birks, 2004). The final age-depth model is given in Figure 7 and shows a narrow 95% confidence interval with a rather constant accumulation rate varying from 0.16 to 0.27 cm/yr and an average of 0.22 cm/yr. AY-RC5, considered to be reworked, does lie within the age range of the modeled curve. Therefore, if reworking occurred, it only comprised recent, shallow material.

4.3.2. Validation by Tephrochronology

Ten layers containing tephra (Table 2 and Figure 7) were sampled and analyzed for their major elements, aiming at relating them to prehistorical eruptions in the area. The result of these analyses are shown in Table S1 in the supporting information and Figure 7, in combination with previous whole-rock and glass shards geochemical data for Mentolat, Macá, Cay and Hudson volcanoes (D'Orazio et al., 2003; Gutiérrez et al., 2005; Haberle & Lumley, 1998; Kratzmann et al., 2009; Naranjo & Stern, 1998). Most of the samples show strong affiliations with products from Hudson Volcano. This volcano has been recurrently active during the Holocene (Naranjo & Stern, 1998; Stern et al., 2016), and probably a number of these eruptions supplied tephra to the fjord, either by direct fall or via the catchment areas of the rivers draining to the fjord. Four of the analyzed tephra layers are attributed to known volcanic eruptions (Table 2). This is in consistence with the age ranges for these layers provided by the age-depth model, and therefore, the volcanic layers are considered to confirm the correctness of the age-depth model.

Sample AY-G3, recovered from a white pumice layer dated at 1,420–1,510 cal years B.P., has been attributed to Macá Volcano, especially given the Ti content being intermediate between those of the Hudson and Mentolat volcanoes. There is only one known eruption for this volcano, and indeed the maximum range given for the MAC1 eruption (1,300–1,520 cal years B.P.) (Naranjo & Stern, 2004) is consistent with the age of this layer. It is not unlikely for material of this eruption to flow into the fjord via either Cuervo River, its catchment comprising Macá Volcano, or Aysén River, of which the catchment was affected by fallout material. This layer has no distinctive signal in the seismic profiles.

The thick pumice interval at about halfway, corresponding to samples AY-G5a and AY-G5b, is represented by SL-E in the seismic profiles (Figure 6d). Its geochemical composition suggests that it was generated by an

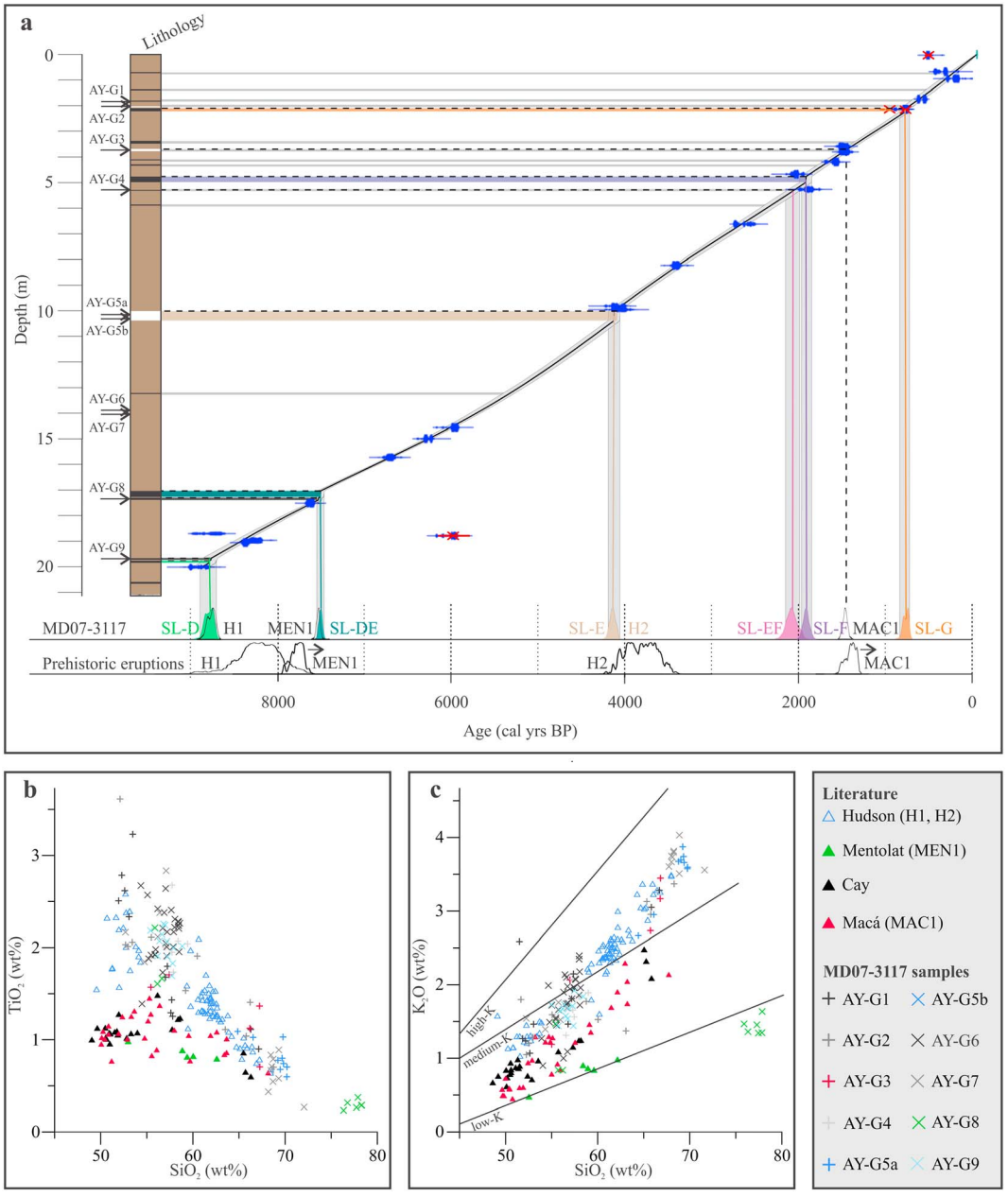

Figure 7. (a) Schematic representation of the core (see Figure 6) with the corresponding age-depth model and correlation of the different events in the core with the seismic data. The colored layers represent the stratigraphic levels identified from the seismic data for which the colors match those from Figure 3. The age-depth model shows a smooth spline curve (black) and the 95% confidence interval (gray), constructed using calibrated radiocarbon ages (blue) taking into account the presence of the instantaneous event deposits. Radiocarbon ages excluded for the construction of the age model are indicated with a red cross. On the age axis, probability density functions for all horizons indicated with a dashed line are given in combination with those cited in literature for prehistorical volcanic eruptions (Naranjo & Stern, 1998, 2004; Stern & Weller, 2012). The age model is validated by tephrochronology (geochemistry samples indicated with black arrows, left), of which the results are presented at the bottom of the figure: (b) TiO_2 versus SiO_2 and (c) K_2O versus SiO_2 with field boundaries after Peccerillo and Taylor (1976); compared to whole-rock composition of Mentolat, Cay, Macá, and Hudson volcanoes. For Hudson, data from volcanic glass is included in the results (D'Orazio et al., 2003; Gutiérrez et al., 2005; Haberle & Lumley, 1998; Kratzmann et al., 2009; Naranjo & Stern, 1998).

Table 2
Age Ranges and Origin of Volcanic Material Present in MD07-3117

Sample number	Core depth (cm)	Origin	Core age (cal years B.P.)	Literature age (cal years B.P.)
AY-G1	178–180	Hudson	580–710	/
AY-G2	199–201	Hudson	670–790	/
AY-G3	375	MAC1	1,420–1,510	<1,300–1,520[a]
AY-G4	530	Hudson	1,980–2,130	/
AY-G5a	1027	H2/SL-E	4,050–4,190	3,460–4,100[b]
AY-G5b	1033			3,970–4,110[c]
AY-G6	1395	Hudson	5,630–5,750	/
AY-G7	1401–1404	Hudson	5,670–5,780	/
AY-G8	1736	MEN1	7,480–7,570	<7,650–7,870[a] 7,630–7,750[d]
AY-G9	1970	H1	8,690–8,860	7,690–8,720[e] 8,410–8,541[d]

[a]Naranjo and Stern (2004). [b]Naranjo and Stern (1998). [c]Van Daele et al. (2016). [d]Stern et al. (2016). [e]Stern and Weller (2012).

eruption of Hudson Volcano. Moreover, seismic amplitudes of this reflector increase toward the Condor River fan, of which the catchment area includes the Hudson Volcano. Considering the thickness and distribution of this volcanic layer throughout the fjord, it is most likely attributed to one of the larger Hudson eruptions (i.e., Ho, H1, or H2; Naranjo & Stern, 1998; Stern et al., 2016; Weller et al., 2014). Because it is the thickest tephra layer in the core and the fact that more pumice was deposited to the north of the volcano (i.e., toward Aysén Fjord) during H2 than during H1 (Naranjo & Stern, 1998), it can be attributed to the H2 eruption. The inferred age model provides an age for this tephra layer between 4,050 and 4,190 cal years B.P., which overlaps with the age of the H2-pumice in Lago Castor of 3,970–4,110 cal years B.P. (Van Daele et al., 2016) and with the age of 3,460–4,100 cal years B.P. given by Naranjo and Stern (1998) (Table 2).

The geochemical composition of AY-G8 (Figure 6e) follows the trend of published onshore compositions from Mentolat Volcano but is characterized by more differentiated, rhyolitic products than the latter (Naranjo & Stern, 2004; Stern et al., 2016). This distinct property is intriguing as there are currently no other data indicating rhyolitic phases from Mentolat. Further analyses are therefore required. However, there is only one known eruption of Mentolat Volcano and therefore we tentatively attribute this layer to the MEN1 eruption. The presence of this tephra can be explained by river supply from Cuervo or Aysén River, as fallout of MEN1 is known to have affected their catchment (Naranjo & Stern, 2004). The age model yields an age range of 7,480–7,570 cal years B.P., consistent with the maximal age of 7,650–7,870 cal years B.P. (Naranjo & Stern, 2004) given for the MEN1 eruption.

Finally, a fourth tephra layer, AY-G9, with a thickness of 6 cm, presents a typical Hudson Volcano geochemical signature. Its considerable thickness allows relating it to one of the larger Holocene Hudson volcanic events and thus most likely H1. The inferred age (8,690–8,860 cal years B.P.) of this tephra layer also matches literature ages published for this eruption of 7,690–8,720 cal years B.P. (Stern & Weller, 2012) and is only slightly older than the average 8,410–8,540 cal years B.P. in lake cores (Stern et al., 2016).

5. Discussion

5.1. Linking Seismic and Sedimentological Data

In order to correlate a stratigraphic level in the seismic profiles with the correct layer in the sediment core, the density of the core was determined by MSCL. Values in the upper 13 m of the core are rather constant, and spikes in density can be correlated to magnetic susceptibility. Therefore, correlation will be based on changes in both density and magnetic susceptibility (Figure 6).

According to the TOPAS profiles, the core was taken just next to an event deposit on SL-E (Figure 3). It is therefore expected that this layer is still rather thick in the core, similar to the maximum vertical resolution of the TOPAS profiles (~30 cm). The only event deposit in this thickness range is the coarse-grained H2 pumice layer halfway down the core of which the top is represented by a trough in the density curve, as can be expected for these low-density grains. Therefore, SL-E—also characterized by increased reflection amplitudes toward the Condor River fan (i.e., inflow from Hudson Volcano)—is assumed to correspond to the H2 pumice layer. For the rest of the correlation, reflection amplitudes and core density and/or MS are compared. The upper

6 m of the core show nine distinct density changes at the event deposits, which correspond to the high-amplitude reflections in the upper ~10 ms of the seismic profile. The lower part of the core shows two small density peaks, which correspond to large peaks in MS. Both peaks can be linked to high reflection amplitudes below SL-E in the seismic profile. The bottom of the core contains high-density rock fragments within a clayey matrix, which can be correlated to the high-amplitude reflections at 0.283 s two-way travel time (TWT) (Figure 6).

The correlation between the sediment core and the seismic records allows inferring the apparent seismic wave velocity along the sedimentary infill of the fjord. Above reflector SL-E, the apparent mean velocity is 1,130 m/s and increases beyond this reflector to 1,310 m/s. Both mean values lie within the range of 1,000 to 2,500 m/s for clay sediments given by Reynolds (2011) but are very low, even lower than the measured bottom-water velocity of 1,506 m/s. This low apparent velocity can be explained by core compaction during retrieval, which is plausible since the core liner was completely filled. A more reasonable velocity of 1,500 m/s (close to the average value of 1,525 m/s measured by MSCL logging in the top 13 m of the core, Figure 6b) would imply a core compaction factor of 1.22, which is less than compaction factors up to 1.3 observed, for example, by Skinner and McCave (2003) for piston cores.

5.2. Event Stratigraphy of Aysén Fjord

The 2007 earthquake is well represented in the seismic reflectors as MTDs and megaturbidites lying on the present-day fjord bottom. The youngest event deposits below 2007 are the SL-G MTDs, which correlate to a 12 cm thick black layer in the core, rich in organic material and interpreted as a turbidite. The synchronicity criterion states that seismically triggered MTDs can be identified by their presence in different locations where they have the same depositional age (Schnellmann et al., 2002). SL-G has multiple landslides in the fjord with different source areas and is thus assumed to be the result of an earthquake. The age range for this deposit is 710–830 cal years B.P. (Figure 7). The organic matter present in the upper centimeters of this deposit was radiocarbon dated (AY-RC5, Table 1) but not included in the construction of the age-depth model since it might be reworked. Nevertheless, its age fits with the one obtained from the model and is therefore assumed to originate from coastal erosion with reworking of recent material only (e.g., by a landslide-induced tsunami wave, as observed during the 2007 earthquake; Lastras et al., 2013; Naranjo et al., 2009).

The following major event deposit is SL-F, with a similar MTD distribution to that from the 2007 event. It corresponds to a thick black turbidite deposit at core depth 476–498 cm (Figure 6c), similar to that generated by the 2007 event (Van Daele et al., 2014) originating from Aysén River Delta failure. Due to these similarities, also SL-F is considered to have been triggered by an earthquake. Similarly to 2007, there might even have been a seismic swarm at the time, with two large shocks spaced so closely in time that they appear to have occurred simultaneously, depositing two MTDs directly on top of each other at the same stratigraphic level (Figure 4). A seismic swarm is, however, not required, and the secondary deposit may also be the result of several other processes such as (i) pressure differences caused by a landslide-induced tsunami wave (as observed by Lastras et al., 2013), (ii) an earthquake only a few years later, (iii) an aseismic trigger mechanism such as heavy rainfall or spontaneous instability after a first shock, or (iv) synchronously triggered mass transport events that reach the location at a different time and do not mix (similar to the 2007 debrites and turbidites; Van Daele et al., 2013). This event took place between 1,850 and 1,980 cal years B.P. (Figure 7).

For SL-EF, its correlative layer in the core is also identified as a thin turbidite based on core logging. Seismic data shows this level holds several small-scale MTDs in different parts of the fjord and is thus interpreted as a level of seismic origin. The age model yields an age between 1,970 and 2,120 cal years B.P. (Figure 7).

The amplitude of the SL-DE reflector, characterized by the presence of MTDs close to the Cuervo Ridge, is rather low at the core location, but a turbidite can be still identified just above the MEN1 tephra (Figure 6e). This means that the Cuervo Ridge MTDs are not the only event deposits present at this level, but another must be located somewhere in an unsurveyed area in the innermost fjord. The turbidite in the core is also composed of dark volcanic sands and could probably originate from the Aysén River Delta, similar to the 2007 sands (Van Daele et al., 2014) and those at SL-F. In any case, the synchronicity criterion is met because event deposits are present at several locations in the fjord and SL-DE is interpreted to be another earthquake-triggered event horizon. The age interval of this level is 7,460–7,540 cal years B.P. (Figure 7).

Finally, SL-D corresponds to a turbidite at 1976–1984 cm depth that seems to consist of two fining upward pulses: a first coarse-grained, granitic pulse separated from a second finer-grained pulse by a sharp

Table 3
Overview of Historical Earthquakes Recorded in Aysén Fjord

Event	Age range (cal years B.P.)	EQ identification criteria	Confidence level seismic trigger
2007	−57	Historical, literature	Certain
SL-G	710–830	Synchronicity	High
SL-F	1,850–1,980	Fault offset, synchronicity, similar to 2007	Very high
SL-EF	1,970–2,120	Synchronicity	High
SL-DE	7,460–7,540	Synchronicity, onshore fault offset	High
SL-D	8,710–8,890	Synchronicity, linked to H1	High
SL-CD	~10,200–10,400	MTD, high-amplitude seismic reflectors	Low
SL-C	~11,300–11,600	MTD, high-amplitude seismic reflectors	Low
SL-B	~12,400–13,000	MTD, high-amplitude seismic reflectors	Medium
SL-A	~18,600–20,000	Synchronicity, high-amplitude seismic reflectors	Medium

transition. These pulses thus originate from different source areas, forming an amalgamated turbidite as was also observed in the 2007 deposits (Van Daele et al., 2014). Having multiple MTDs in different areas in the fjord combined with an amalgamated turbidite in the core, they are very likely triggered by an earthquake. The level is dated to 8,710–8,890 cal years B.P. (Figure 7).

Four additional stratigraphic layers (SL-CD, SL-C, SL-B, and SL-A) have been identified on the seismic profiles but were not reached by coring. This only allows making assumptions about these events, and no conclusions can be made with certainty. Taking into account a constant sedimentation rate of 0.22 cm/yr, the age for SL-CD would be about 10,400 cal years B.P., 11,600 cal years B.P. for SL-C, 13,000 cal years B.P. for SL-B, and 20,000 cal years B.P. for SL-A, which is much older than the first estimates made by Van Daele et al. (2013) without the availability of a dated long sediment core. Nevertheless, it needs to be considered that below SL-CD, the seismic facies changes with a higher frequency of high-amplitude reflectors (Figure 3), which could indicate a change in sedimentation rate. However, Lago Castor (located at a similar latitude) shows sedimentation rates that remain more or less constant up to the Ho eruption (Van Daele et al., 2016). A slight increase to, for example, 0.25 cm/yr would give an age of about 17,300 cal years B.P. for the formation of the Condor River fan (Figure 3). This indicated that it might be attributed to the recently discovered Ho eruption (Weller et al., 2014) rather than to H1 as postulated by Van Daele et al. (2013). The origin of these four event levels cannot be stated with certainty, but the fact that a high-amplitude reflector is present over the entire fjord for all four levels (indicating the presence of a widespread turbidite) and that over the entire 8,000 years present in the core every slope failure event from the seismic profiles can be interpreted as being seismically triggered, there is no reason to assume that this would be any different for the remaining stratigraphic levels. A summarizing table with all prehistorical earthquakes in the Aysén region and their ages is given in Table 3.

5.3. Linking MTD Events With Source Faults

5.3.1. Liquiñe-Ofqui Fault Zone

The large fault to the northwest in Figure 3 is interpreted as the offshore continuation of the Quitralco Fault (Figure 5). As this fault hosted the main shock of the 2007 seismic swarm and there is a vertical offset at the seafloor, this is interpreted as the result of the 2007 earthquake. Apart from the 2007 earthquake, the earthquake that generated MTDs on SL-F must also have taken place along the Quitralco Fault, as demonstrated by the offset change along the fault at the SL-F horizon (Figure 5). The SL-F horizon is offset 5 ms (or 3 ms coseismic offset if we discount the seafloor offset accumulated by the 2007 event), but the earthquake-generated megaturbidite ponds in the northwestern "downthrown" fault block (similar to observations of Marco & Agnon, 1995 in the Dead Sea graben), reducing the offset to 2 ms (or leveling the offset, if we discount the 2007 displacement). However, these reflector offsets cannot be directly related to the actual vertical fault offset of the bedrock fault, which is assumed to be negligible for a pure strike-slip focal mechanism (Figure 5). The observed fault in the fjord's sedimentary infill is the result of deformation of the sedimentary infill in response to the strike-slip movement of the bedrock (e.g., Brothers et al., 2011; de La Taille et al., 2015; Van Daele et al., 2011), which can include, among others, Riedel shear fractures and extension fractures (Cloos, 1932; Sylvester, 1988). While the central part of the observed fault (where no vertical offset is observed) has an orientation parallel to the bedrock fault, the orientation of the fault at its northern and southern extremes (where the vertical offset is observed) tends to that expected for extension fractures. Hence, the

observed vertical offset is the result of subsidence due to extension, which can indeed be expected for the observed fault orientation (Figure 5). The observed fault in the sediments is thus consistent with a "surface" rupture of the bedrock below the fjord's sedimentary infill, which may even have been larger for SL-F than during the 2007 earthquake considering the larger vertical offset.

The direct evidence of a Quitralco Fault surface rupture below the fjord for both the SL-F and 2007 events is an important observation that supports the use of synchronous MTDs in paleoseismic records. Moreover, as the MTD distributions in the fjord of SL-F and 2007 are very similar (Figure 4), we argue that the distribution may actually be used to estimate the ruptured fault segment for an earthquake that triggered MTDs.

The rupture responsible for the SL-F event may even have extended more to the north of the fjord, where Vargas et al. (2013) obtained a maximum age of 7,750–8,500 cal years B.P. for faulting of deltaic sediments at the southern end of the Cuervo River Delta (white dot, Figure 5). Alternatively, the observed faulting may be responsible for the SL-DE event (7,460–7,540 cal years B.P.). In that case, the fault rupture must have been restricted to the trace north of the fjord as we do not observe offset in the fjord sediments associated to this event. This would also be consistent with the MTD distribution of SL-DE, that is, in the northern part of the fjord, close to the Quitralco Fault, although more abundant MTDs would be expected for an earthquake with such a nearby surface rupture.

Although no direct rupture evidence is available for any of the other MTD events, we can hypothesize on responsible faults in the vicinity of the fjord based on the MTD distributions taking into account that seismic intensities of crustal earthquakes diminish rapidly with increasing distance to the source (Bakun & Wentworth, 1997), as was also observed during the 2007 earthquake (Naranjo et al., 2009). The large MTD of SL-B at the foot of the Cuervo River Delta may indicate an earthquake on the Quitralco Fault, somewhere north of the fjord, similar to SL-DE. The more easterly distribution of MTDs for SL-A, SL-C, and SL-G may indicate an earthquake on a fault to the east of the Quitralco Fault, such as the Liquiñe-Ofqui Main Fault or the Azul-Tigre Fault (Figure 1). Finally, the southern location of the MTDs of SL-CD and SL-D indicates an earthquake source to the south of the fjord, with also the Liquiñe-Ofqui Main Fault, the Azul-Tigre Fault, or even the Río Mañihuales Fault as main potential source faults. Thomson (2002) found that these last two were active at multiple occasions during the Late Miocene and Pliocene.

5.3.2. Megathrust Earthquakes

The widespread, small-scale MTDs of SL-EF may be the result of an earthquake along the Chilean subduction zone. Subduction earthquake ruptures are located relatively far away from the study area and would lead to an almost uniform seismic intensity in the fjord. For the last two major megathrust earthquakes in Chile (1960 and 2010) Van Daele et al. (2015) report seismic intensities up to VII½–VIII in lakes situated at about the same distance from the subduction zone as Aysén Fjord, but located more to the north. Since the northern part of the Valdivia segment is currently locked (Moreno et al., 2011), maximal slip is expected in the north, as was the case during the 1960 Great Chilean earthquake. Lazo Hinrichs (2008) report seismic intensities of IV in Puerto Aysén for this megathrust earthquake, which did not trigger any landslides in the fjord. However, should a large amount of slip occur at the latitude of Aysén Fjord, an intensity of VII½–VIII could be regarded as a maximum seismic intensity in the fjord for subduction earthquakes in accordance with observations by Van Daele et al. (2015), where this value is reported for the largest earthquake on record. Nevertheless, an intensity of VII½–VIII is still considerably lower than local intensities up to IX for a LOFZ earthquake and probably unable to trigger onshore landslides (Howarth et al., 2014). We can thus readily expect widespread offshore-originating small-scale MTDs for a megathrust earthquake with high slip ($>$ 30 m) in the southern part of the Valdivia segment. As such, we argue that SL-EF (1,970–2,120 cal years B.P.) can be correlated to the tsunami deposit of event hI in coastal Lake Huelde on Chiloé Island (1,903–2,006 cal years B.P.) (Kempf et al., 2017) and to a turbidite in Lake Riñihue (1,929–2,103 cal years B.P.) (Moernaut et al., 2018). This earthquake caused intensities of VI½ $<$ VII½ at the latter study site, which is less than intensities of $\geq$VII½ for the largest earthquakes on the northern part of the Valdivia segment. Combined with the presence of tsunami deposits in the southern part of the segment (Kempf et al., 2017) and our SL-EF, we infer this to be an (exceptional) earthquake with a large amount of slip in the southern part of the Valdivia segment and less slip in the northern part.

5.3.3. Earthquake History of Aysén Fjord

Based on the data presented above, we can conclude that only one Holocene megathrust earthquake (about 2,000 cal years B.P.) was strong enough to destabilize the Aysén Fjord area, intensities up to VII½. Other

significant earthquakes in the area are related to activity along the LOFZ and occurred on average once every 2,100 years during the Holocene. However, earthquake clusters seem to occur during the early and late Holocene, with an interval of around 1,200 years in between successive earthquakes in contrast to a calm period during the middle Holocene. The major source of seismic hazard for the Aysén region thus originates from the LOFZ. To better understand hazard in the region, ground motion modeling is required to provide constraints on the causative faults, as well as additional (dated) records from fjords and/or lakes.

5.4. Cascading Events: Possible Link Between Seismic and Volcanic Activity

The 2007 seismic swarm has been interpreted as driven by ascending fluids (Legrand et al., 2011), resulting in activation of the LOFZ and two $M_w > 6$ earthquakes. This swarm thus clearly illustrates the potential causal relationship between volcanic and seismic activity in the study area, as is also postulated by Vargas et al. (2013). Our paleo-event record indicates that such cascading events may indeed have occurred throughout the history of the LOFZ. The MTDs at SL-D were triggered in the southernmost part of Aysén Fjord and thus hint to an earthquake source south of the fjord, toward Hudson Volcano. As this earthquake preceded the major Hudson H1 eruption by a short period (up to maximum a few decades), there may indeed be a causal relation between both events. This thus confirms the conclusions by Agurto-Detzel et al. (2014), who argued that high-magnitude earthquakes can be related to eruptive phases of the Hudson Volcano.

Similarly, the MEN1 eruption and the SL-DE earthquake may have a causal relation, as these events also occurred in a similar short time period than SL-D and H1. However, the SL-DE earthquake is likely hosted by the Quitralco Fault not too far north of the fjord, which seems rather far away from the Mentolat Volcano (~75 km to the north) to have a causal relationship.

6. Conclusion

This study illustrates that fjords can be an excellent setting to perform paleoseismological studies based on the deposition of multiple synchronous landslides. Seismic profiling and a long sediment core in Aysén Fjord have revealed 10 stratigraphic levels on which MTDs are present and are related to seismic activity, together with four volcanic tephra layers that can be linked to major Holocene eruptions from different volcanoes in the Andean Southern Volcanic Zone, including Hudson, Mentolat, and Macá. Six of the identified stratigraphic levels are interpreted as the definite result of major Holocene earthquakes related to the Liquiñe-Ofqui Fault Zone (LOFZ) with a rough estimate of one earthquake every 2,100 years and clusters occurring during the early and late Holocene. The LOFZ is thus the main source of seismic hazard in the Aysén region. Moreover, one of these stratigraphic levels could be correlated to fault offset observed on the seismic profiles. Another stratigraphic level has been interpreted as the result of a megathrust earthquake occurring at around 2,000 cal years B.P. and can be linked to a tsunami deposit and a turbidite in lakes more to the north. Possibly four additional late and pre-Holocene earthquakes that affected Aysén Fjord are recorded in the sedimentary sequence. Finally, we found that a causal relationship between earthquakes and volcanic eruptions is likely a returning phenomenon along the LOFZ. The outlook of this research includes modeling of the seismically induced ground motions to yield better constraints on the magnitude and faults that ruptured for historical earthquakes. Our findings could be confirmed by comparable studies in other fjords and/or lakes in the region.

Acknowledgments
This research was funded mainly by the Fund for Scientific Research Flanders (FWO-Vlaanderen), the Spanish project DETSUFA (CTM2010-09891-E), and a Catalan Government Grups de Recerca Consolidats grant (2014 SGR 1068). We are grateful to the PACHIDERME, DETSUFA, and RV *Don Este* crews. We thank R. Achten for the use of the CT scanner in Ghent University Hospital. We also thank the Laboratoire de Mesures Carbone 14 (LMC14) in Saclay (France) for handling the radiocarbon dating with Artemis, and Philipp Kempf for his assistance in creating a suitable age-depth model. We thank Jasper Moernaut for proofreading an earlier version of this manuscript. Two anonymous reviewers are acknowledged for detailed reviews, which improved the manuscript. IHS Kingdom Suite is acknowledged for their educational user license providing seismic interpretation software. Seismic, multibeam, and other supporting information are available upon request to the authors.

References

Agurto-Detzel, H., Rietbrock, A., Bataille, K., Miller, M., Iwamori, H., & Priestley, K. (2014). Seismicity distribution in the vicinity of the Chile Triple Junction, Aysén region, southern Chile. *Journal of South American Earth Sciences*, *51*, 1–11. https://doi.org/10.1016/j.jsames.2013.12.011

Bakun, W. u., & Wentworth, C. (1997). Estimating earthquake location and magnitude from seismic intensity data. *Bulletin of the Seismological Society of America*, *87*(6), 1502–1521.

Barrientos, S. E., & Ward, S. N. (1990). The 1960 Chile earthquake: Inversion for slip distribution from surface deformation. *Geophysical Journal International*, *103*(3), 589–598. https://doi.org/10.1111/j.1365-246X.1990.tb05673.x

Beck, C. (2009). Late Quaternary lacustrine paleo-seismic archives in north-western Alps: Examples of earthquake-origin assessment of sedimentary disturbances. *Earth-Science Reviews*, *96*, 327–344. https://doi.org/10.1016/j.earscirev.2009.07.005

Bertrand, S., Araneda, A., Vargas, P., Jana, P., Fagel, N., & Urrutia, R. (2012). Using the N/C ratio to correct bulk radiocarbon ages from lake sediments: Insights from Chilean Patagonia. *Quaternary Geochronology*, *12*, 23–29. https://doi.org/10.1016/j.quageo.2012.06.003

Bertrand, S., Daga, R., Bedert, R., & Fontijn, K. (2014). Deposition of the 2011–2012 Cordón Caulle tephra (Chile, 40 S) in lake sediments: Implications for tephrochronology and volcanology. *Journal of Geophysical Research: Earth Surface*, *119*, 2555–2573.

Björck, S., Bennike, O., Possnert, G., Wohlfarth, B., & Digerfeldt, G. (1998). A high-resolution ^{14}C dated sediment sequence from southwest Sweden: Age comparisons between different components of the sediment. *Journal of Quaternary Science*, *13*(1), 85–89. https://doi.org/10.1002/(SICI)1099-1417(199801/02)13:1%3C85::AID-JQS360%3E3.0.CO;2-S

Blaauw, M. (2010). Methods and code for "classical" age-modelling of radiocarbon sequences. *Quaternary Geochronology*, *5*, 512–518. https://doi.org/10.1016/j.quageo.2010.01.002

Bøe, R., Longva, O., Lepland, A., Blikra, L. H., Sonstegaard, E., Haflidason, H., … Lien, R. (2004). Postglacial mass movements and their causes in fjords and lakes in western Norway. *Norsk Geologisk Tidsskrift*, *84*, 35–56.

Brothers, D., Kilb, D., Luttrell, K., Driscoll, N., & Kent, G. (2011). Loading of the San Andreas fault by flood-induced rupture of faults beneath the Salton Sea. *Nature Geoscience*, *4*, 486–492. https://doi.org/10.1038/ngeo1184

Carel, M., Siani, G., & Delpech, G. (2011). Tephrostratigraphy of a deep-sea sediment sequence off the south Chilean margin: New insight into the Hudson volcanic activity since the last glacial period. *Journal of Volcanology and Geothermal Research*, *208*, 99–111. https://doi.org/10.1016/j.jvolgeores.2011.09.011

Carrillo, E., Beck, C., Audemard, F. A., Moreno, E., & Ollarves, R. (2008). Disentangling late Quaternary climatic and seismo-tectonic controls on Lake Mucubají sedimentation (Mérida Andes, Venezuela). *Palaeogeography, Palaeoclimatology, Palaeoecology*, *259*, 284–300. https://doi.org/10.1016/j.palaeo.2007.10.012

Cembrano, J., Hervé, F., & Lavenu, A. (1996). The Liquiñe Ofqui fault zone: A long-lived intra-arc fault system in southern Chile. *Tectonophysics*, *259*(1-3), 55–66. https://doi.org/10.1016/0040-1951(95)00066-6

Cembrano, J., & Lara, L. (2009). The link between volcanism and tectonics in the southern volcanic zone of the Chilean Andes: A review. *Tectonophysics*, *471*, 96–113. https://doi.org/10.1016/j.tecto.2009.02.038

Cembrano, J., Schermer, E., Lavenu, A., & Sanhueza, A. (2000). Contrasting nature of deformation along an intra-arc shear zone, the Liquiñe–Ofqui fault zone, southern Chilean Andes. *Tectonophysics*, *319*(2), 129–149. https://doi.org/10.1016/S0040-1951(99)00321-2

Cifuentes, I. L. (1989). The 1960 Chilean earthquakes. *Journal of Geophysical Research*, *94*(B1), 665–680. https://doi.org/10.1029/JB094iB01p00665

Cisternas, M., Atwater, B. F., Torrejón, F., Sawai, Y., Machuca, G., Lagos, M., … Husni, M. (2005). Predecessors of the giant 1960 Chile earthquake. *Nature*, *437*, 404–407. https://doi.org/10.1038/nature03943

Cisternas, M., Garrett, E., Wesson, R., Dura, T., & Ely, L. L. (2017). Unusual geologic evidence of coeval seismic shaking and tsunamis shows variability in earthquake size and recurrence in the area of the giant 1960 Chile earthquake. *Marine Geology*, *385*, 101–113. https://doi.org/10.1016/j.margeo.2016.12.007

Cloos, E. (1932). "Feather joints" as indicators of the direction of movements on faults, thrusts, joints and magmatic contacts. *Proceedings of the National Academy of Sciences*, *18*(5), 387–395. https://doi.org/10.1073/pnas.18.5.387

de La Taille, C., Jouanne, F., Crouzet, C., Beck, C., Jomard, H., de Rycker, K., & Van Daele, M. (2015). Impact of active faulting on the post LGM infill of Le Bourget Lake (western Alps, France). *Tectonophysics*, *664*, 31–49. https://doi.org/10.1016/j.tecto.2015.08.024

D'Orazio, M., Innocenti, F., Manetti, P., Tamponi, M., Tonarini, S., González-Ferrán, O., … Omarini, R. (2003). The Quaternary calc-alkaline volcanism of the Patagonian Andes close to the Chile triple junction: Geochemistry and petrogenesis of volcanic rocks from the Cay and Maca volcanoes (~45°S, Chile). *Journal of South American Earth Sciences*, *16*(4), 219–242. https://doi.org/10.1016/S0895-9811(03)00063-4

Gutiérrez, F., Gioncada, A., González Ferran, O., Lahsen, A., & Mazzuoli, R. (2005). The Hudson volcano and surrounding monogenetic centres (Chilean Patagonia): An example of volcanism associated with ridge–trench collision environment. *Journal of Volcanology and Geothermal Research*, *145*, 207–233. https://doi.org/10.1016/j.jvolgeores.2005.01.014

Haberle, S. G., & Lumley, S. H. (1998). Age and origin of tephras recorded in postglacial lake sediments to the west of the southern Andes, 44°S to 47°S. *Journal of Volcanology and Geothermal Research*, *84*(3-4), 239–256. https://doi.org/10.1016/S0377-0273(98)00037-7

Hervé, M. (1976). Estudio geológico de la Falla Liquiñe-Reloncaví en el área de Liquiñe: Antecedentes de un movimiento transcurrente (Provincia de Valdivia), paper presented at I Congreso Geológico Chileno, Santiago.

Hogg, A. G., Hua, Q., Blackwell, P. G., Niu, M., Buck, C. E., Guilderson, T. P., … Reimer, R. W. (2013). SHCal13 Southern Hemisphere calibration, 0–50,000 years cal BP. *Radiocarbon*, *55*(04), 1889–1903. https://doi.org/10.2458/azu_js_rc.55.16783

Howarth, J. D., Fitzsimons, S. J., Norris, R. J., & Jacobsen, G. E. (2014). Lake sediments record high intensity shaking that provides insight into the location and rupture length of large earthquakes on the Alpine Fault, New Zealand. *Earth and Planetary Science Letters*, *403*, 340–351. https://doi.org/10.1016/j.epsl.2014.07.008

Kempf, P., Moernaut, J., Van Daele, M., Vandoorne, W., Pino, M., Urrutia, R., & De Batist, M. (2017). Coastal lake sediments reveal 5500 years of tsunami history in south central Chile. *Quaternary Science Reviews*, *161*, 99–116. https://doi.org/10.1016/j.quascirev.2017.02.018

Kissel, C., Leau, H., & The Shipboard Scientific party (2007). MD159-PACHIDERME-IMAGES XV, cruise report.*Rep*., 105 pp, Institut Paul-Emile Victor.

Kratzmann, D. J., Carey, S., Scasso, R., & Naranjo, J.-A. (2009). Compositional variations and magma mixing in the 1991 eruptions of Hudson volcano, Chile. *Bulletin of Volcanology*, *71*.

Kremer, K., Wirth, S. B., Reusch, A., Fäh, D., Bellwald, B., Anselmetti, F. S., … Strasser, M. (2017). Lake-sediment based paleoseismology: Limitations and perspectives from the Swiss Alps. *Quaternary Science Reviews*, *168*, 1–18. https://doi.org/10.1016/j.quascirev.2017.04.026

Lastras, G., Amblas, D., Calafat, A. M., Canals, M., Frigola, J., Hermanns, R. L., … Rayo, X. (2013). Landslides cause tsunami waves: Insights from Aysén fjord, Chile. *Eos*, *94*(34), 297–298. https://doi.org/10.1002/2013EO340002

Lastras, G., & The Shipboard Scientific Party (2013). DETSUFA Cruise Report. *Rep*., CRG Marine Geosciences, University of Barcelona (UB), Barcelona, Spain.

Lazo Hinrichs, R. G. (2008). Estudio de los daños de los terremotos del 21 y 22 de Mayo de 1960, Memoria para optar al título de Igeniero Civil thesis, 427 pp, Universidad de Chile, Santiago, Chile.

Legrand, D., Barrientos, S., Bataille, K., Cembrano, J., & Pavez, A. (2011). The fluid-driven tectonic swarm of Aysen Fjord, Chile (2007) associated with two earthquakes ($M_w = 6.1$ and $M_w = 6.2$) within the Liquiñe-Ofqui fault zone. *Continental Shelf Research*, *31*, 154–161. https://doi.org/10.1016/j.csr.2010.05.008

Lomnitz, C. (2004). Major earthquakes of Chile: A historical survey, 1535–1960. *Seismological Research Letters*, *75*, 368–378. https://doi.org/10.1785/gssrl.75.3.368

Marco, S., & Agnon, A. (1995). Prehistoric earthquake deformations near Masada, Dead Sea graben. *Geology*, *23*(8), 695–698. https://doi.org/10.1130/0091-7613(1995)023%3C0695:PEDNMD%3E2.3.CO;2

McHugh, C., Seeber, L., Cormier, M., Dutton, J., Cagatay, N., Polonia, A., … Gorur, N. (2006). Submarine earthquake geology along the north Anatolia fault in the Marmara Sea, Turkey: A model for transform basin sedimentation. *Earth and Planetary Science Letters*, *248*, 661–684. https://doi.org/10.1016/j.epsl.2006.05.038

Melnick, D., Bookhagen, B., Strecker, M. R., & Echtler, H. P. (2009). Segmentation of megathrust rupture zones from fore-arc deformation patterns over hundreds to millions of years, Arauco peninsula, Chile. *Journal of Geophysical Research*, *114* B01407. https://doi.org/10.1029/2008JB005788

Moernaut, J., De Batist, M., Charlet, F., Heirman, K., Chapron, E., Pino, M., … Urrutia, R. (2007). Giant earthquakes in south-central Chile revealed by Holocene mass-wasting events in Lake Puyehue. *Sedimentary Geology*, *195*, 239–256. https://doi.org/10.1016/j.sedgeo.2006.08.005

Moernaut, J., Van Daele, M., Fontijn, K., Heirman, K., Kempf, P., Pino, M., … De Batist, M. (2018). Larger earthquakes recur more periodically: New insights in the megathrust earthquake cycle from lacustrine turbidite records in south-central Chile. *Earth and Planetary Science Letters*, *481*, 9–19. https://doi.org/10.1016/j.epsl.2017.10.016

Moernaut, J., Van Daele, M., Heirman, K., Fontijn, K., Strasser, M., Pino, M., … De Batist, M. (2014). Lacustrine turbidites as a tool for quantitative earthquake reconstruction: New evidence for a variable rupture mode in south central Chile. *Journal of Geophysical Research: Solid Earth*, *119*, 1607–1633.

Monecke, K., Anselmetti, F. S., Becker, A., Sturm, M., & Giardini, D. (2004). The record of historic earthquakes in lake sediments of Central Switzerland. *Tectonophysics*, *394*, 21–40. https://doi.org/10.1016/j.tecto.2004.07.053

Mora, C., Comte, D., Russo, R., Gallego, A., & Mocanu, V. (2010). Aysén seismic swarm (January 2007) in southern Chile: Analysis using joint hypocenter determination. *Journal of Seismology*, *14*, 683–691. https://doi.org/10.1007/s10950-010-9190-y

Moreau, C., Caffy, I., Comby, C., Delqué-Količ, E., Dumoulin, J. P., Hain, S., … Vincent, J. (2013). Research and development of the Artemis ^{14}C AMS Facility: Status report. *Radiocarbon*, *55*(02), 331–337. https://doi.org/10.1017/S0033822200057441

Moreno, M., Bolte, J., Klotz, J., & Melnick, D. (2009). Impact of megathrust geometry on inversion of coseismic slip from geodetic data: Application to the 1960 Chile earthquake. *Geophysical Research Letters*, *36*, L16310. https://doi.org/10.1029/2009GL039276

Moreno, M., Melnick, D., Rosenau, M., Bolte, J., Klotz, J., Echtler, H., … Oncken, O. (2011). Heterogeneous plate locking in the south–central Chile subduction zone: Building up the next great earthquake. *Earth and Planetary Science Letters*, *305*, 413–424. https://doi.org/10.1016/j.epsl.2011.03.025

Naranjo, J. A., Arenas, M., Clavero, J., & Munoz, O. (2009). Mass movement-induced tsunamis: Main effects during the Patagonian Fjordland seismic crisis in Aisén (45° 25′S), Chile. *Andean Geology*, *36*, 137–146-145.

Naranjo, J. A., & Stern, C. R. (1998). Holocene explosive activity of Hudson volcano, southern Andes. *Bulletin of Volcanology*, *59*(4), 291–306. https://doi.org/10.1007/s004450050193

Naranjo, J. A., & Stern, C. R. (2004). Holocene tephrochronology of the southernmost part (42°30′–45°S) of the Andean southern volcanic zone. *Revista Geologica de Chile*, *31*, 224–240.

Peccerillo, A., & Taylor, S. R. (1976). Geochemistry of Eocene calc-alkaline volcanic rocks from the Kastamonu area, northern Turkey. *Contributions to Mineralogy and Petrology*, *58*(1), 63–81. https://doi.org/10.1007/BF00384745

Praet, N., Moernaut, J., Van Daele, M., Boes, E., Haeussler, P. J., Strupler, M., … De Batist, M. (2017). Paleoseismic potential of sublacustrine landslide records in a high-seismicity setting (south-central Alaska). *Marine Geology*, *384*, 103–119. https://doi.org/10.1016/j.margeo.2016.05.004

Reynolds, J. M. (2011). *An Introduction to Applied and Environmental Geophysics* (2nd ed.). Chichester, UK: Wiley-Blackwell.

Russo, R. M., Gallego, A., Comte, D., Mocanu, V. I., Murdie, R. E., Mora, C., & VanDecar, J. C. (2011). Triggered seismic activity in the Liquiñe-Ofqui fault zone, southern Chile, during the 2007 Aysen seismic swarm. *Geophysical Journal International*, *184*, 1317–1326. https://doi.org/10.1111/j.1365-246X.2010.04908.x

Salamanca, M. A., & Jara, B. (2003). Distribución y acumulación de plomo (Pb y ^{210}Pb) en sedimentos de los fiordos de la XI región. Chile. *Ciencia y Tecnología del Mar*, *26*(2), 61–71.

Schnellmann, M., Anselmetti, F. S., Giardini, D., McKenzie, J. A., & Ward, S. N. (2002). Prehistoric earthquake history revealed by lacustrine slump deposits. *Geology*, *30*(12), 1131–1134. https://doi.org/10.1130/0091-7613(2002)030%3C1131:PEHRBL%3E2.0.CO;2

Sepúlveda, S. A., Serey, A., Lara, M., Pavez, A., & Rebolledo, S. (2010). Landslides induced by the April 2007 Aysén Fjord earthquake, Chilean Patagonia. *Landslides*, *7*, 483–492. https://doi.org/10.1007/s10346-010-0203-2

Sernageomin (2002). Mapa geológico de Chile: Versión digital, escala 1:1.000.000, edited, Santiago, Chile.

Skinner, L. C., & McCave, I. N. (2003). Analysis and modelling of gravity- and piston coring based on soil mechanics. *Marine Geology*, *199*(1-2), 181–204. https://doi.org/10.1016/S0025-3227(03)00127-0

Stern, C. R. (2004). Active Andean volcanism: Its geologic and tectonic setting. *Revista Geologica de Chile*, *31*, 161–206.

Stern, C. R., Moreno, P. I., Henríquez, W. I., Villa-Martínez, R., Sagredo, E., Aravena, J. C., & de Pol-Holz, R. D. (2016). Holocene tephrochronology around Cochrane (~ 47 S), southern Chile. *Andean Geology*, *43*(1).

Stern, C. R., & Weller, D. (2012). A revised age of 7430±250 ^{14}C yrs BP for the very large mid-Holocene explosive H1 eruption of the Hudson volcano, Southern Chile, paper presented at 13th Chilean Geologic Congress, Antofagasta, Chile (2 pp.).

St-Onge, G., Chapron, E., Mulsow, S., Salas, M., Viel, M., Debret, M., … Locat, J. (2012). Comparison of earthquake-triggered turbidites from the Saguenay (eastern Canada) and Reloncavi (Chilean margin) fjords: Implications for paleoseismicity and sedimentology. *Sedimentary Geology*, *243-244*, 89–107. https://doi.org/10.1016/j.sedgeo.2011.11.003

Strasser, M., Anselmetti, F. S., Fäh, D., Giardini, D., & Schnellmann, M. (2006). Magnitudes and source areas of large prehistoric northern alpine earthquakes revealed by slope failures in lakes. *Geology*, *34*, 1005. https://doi.org/10.1130/G22784A.1

Sylvester, A. G. (1988). Strike-slip faults. *Geological Society of America Bulletin*, *100*(11), 1666–1703. https://doi.org/10.1130/0016-7606(1988)100<1666:SSF>2.3.CO;2

Telford, R. J., Heegaard, E., & Birks, H. J. B. (2004). All age–depth models are wrong: But how badly? *Quaternary Science Reviews*, *23*, 1–5. https://doi.org/10.1016/j.quascirev.2003.11.003

Thomson, S. N. (2002). Late Cenozoic geomorphic and tectonic evolution of the Patagonian Andes between latitudes 42°S and 46°S: An appraisal based on fission-track results from the transpressional intra-arc Liquiñe-Ofqui fault zone. *GSA Bulletin*, *114*(9), 1159–1173.

Törnqvist, T. E., De Jong, A. F., Oosterbaan, W. A., & Van Der Borg, K. (1992). Accurate dating of organic deposits by AMS ^{14}C measurement of macrofossils. *Radiocarbon*, *34*(03), 566–577. https://doi.org/10.1017/S0033822200063840

Van Daele, M., Bertrand, S., Meyer, I., Moernaut, J., Vandoorne, W., Siani, G., … d. B. M. (2016). Late Quaternary evolution of Lago Castor (Chile, 45.6°S): Timing of the deglaciation in northern Patagonia and evolution of the southern westerlies during the last 17 kyr. *Quaternary Science Reviews*, *133*, 130–146. https://doi.org/10.1016/j.quascirev.2015.12.021

Van Daele, M., Cnudde, V., Duyck, P., Pino, M., Urrutia, R., De Batist, M., & Trofimovs, J. (2014). Multidirectional, synchronously-triggered seismo-turbidites and debrites revealed by X-ray computed tomography (CT). *Sedimentology*, *61*(4), 861–880. https://doi.org/10.1111/sed.12070

Van Daele, M., Moernaut, J., Doom, L., Boes, E., Fontijn, K., Heirman, K., … de Batist, M. (2015). A comparison of the sedimentary records of the 1960 and 2010 great Chilean earthquakes in 17 lakes: Implications for quantitative lacustrine palaeoseismology, *Sedimentology*, *62*(5), 1466–1496. https://doi.org/10.1111/sed.12193

Van Daele, M., Van Welden, A., Moernaut, J., Beck, C., Audemard, F., Sanchez, J., … Lemus, A. (2011). Reconstruction of late-Quaternary sea-and lake-level changes in a tectonically active marginal basin using seismic stratigraphy: The Gulf of Cariaco, NE Venezuela. *Marine Geology*, *279*, 37–51. https://doi.org/10.1016/j.margeo.2010.10.011

Van Daele, M., Versteeg, W., Pino, M., Urrutia, R., & De Batist, M. (2013). Widespread deformation of basin-plain sediments in Aysén fjord (Chile) due to impact by earthquake-triggered, onshore-generated mass movements. *Marine Geology*, *337*, 67–79. https://doi.org/10.1016/j.margeo.2013.01.006

Vargas, G., Rebolledo, S., Sepúlveda, S. A., Lahsen, A., Thiele, R., Townley, B., … Lara, M. (2013). Submarine earthquake rupture, active faulting and volcanism along the major Liquiñe-Ofqui Fault Zone and implications for seismic hazard assessment in the Patagonian Andes. *Andean Geology*, *40*(1).

Waldmann, N., Anselmetti, F. S., Ariztegui, D., Austin, J. A. Jr., Pirouz, M., Moy, C. M., & Dunbar, R. (2011). Holocene mass-wasting events in Lago Fagnano, Tierra del Fuego (54°S): Implications for paleoseismicity of the Magallanes-Fagnano transform fault. *Basin Research*, *23*, 171–190. https://doi.org/10.1111/j.1365-2117.2010.00489.x

Wang, K., Hu, Y., Bevis, M., Kendrick, E., Smalley, R., Vargas, R. B., & Lauría, E. (2007). Crustal motion in the zone of the 1960 Chile earthquake: Detangling earthquake-cycle deformation and forearc-sliver translation. *Geochemistry, Geophysics, Geosystems*, *8*, Q10010.

Weller, D., Miranda, C. G., Moreno, P. I., Villa-Martínez, R., & Stern, C. R. (2014). The large late-glacial Ho eruption of the Hudson volcano, southern Chile. *Bulletin of Volcanology*, *76*(6). https://doi.org/10.1007/s00445-014-0831-9